Fast and Efficient Adaptation Algorithms for Multi-Gigabit Wireless Infrared Systems

Fuad E. Alsaadi, Mohammed A. Alhartomi, and Jaafar M. H. Elmirghani, *Senior Member, IEEE*

***Abstract*—Multibeam angle adaptive systems (MBAAS) have been shown to offer performance improvements over traditional spot-diffusing optical wireless systems. However, an increase in the computational cost is incurred. This paper introduces a method to speed up the adaptation process through efficient use of a divide and conquer algorithm by recursively breaking down the scanning process and focusing it into a smaller region in each iteration. The new, fast and efficient angle adaptation algorithm offers the advantages of optimizing the number and pattern (positions) of the spots so as to maximize the receiver's signal-to-noise ratio (SNR), regardless of the transmitter's position, the receiver's orientation and its field of view. It can also adapt to environmental changes, providing a robust link against shadowing and signal blockage. Furthermore, a beam delay adaptation method is used to reduce the effect of multipath dispersion and inter-symbol interference. The combination of angle and delay adaptation adds a degree of freedom to the link design, resulting in a compact impulse response and a system that is able to achieve higher data rates (15 Gbit/s). Significant improvements in the SNR, with optical wireless channel bandwidths of more than 15 GHz are obtained, and eye safety is considered while operating at 15 Gbit/s with full mobility in a realistic environment where shadowing exists.**

***Index Terms*—Beam angle adaptation, beam delay adaptation, diversity receiver, high-speed optical wireless communication, transmit power adaptation.**

I. Introduction

INFRARED (IR) wireless communication offers a number of potential advantages over its radio frequency counterpart. The advantages include the potential for high-speed communications, freedom from fading [1], as well as freedom from spectrum regulations and licensing. IR links provide immunity from electromagnetic interference and allow the use of inexpensive optoelectronic devices [1]. They also offer a degree of security at the physical layer and prevent interference between links operating in different rooms. The two major impairments of wireless IR links include background noise (BN) attributed to natural and artificial light sources and multipath propagation. The former degrades the SNR, while the latter limits the maximum achievable data rate. In addition, the maximum allowed optical power is restricted by eye and skin safety regulations [2]–[4].

IR wireless links are often categorized into two basic schemes: direct line-of-sight (LOS) and diffuse systems. Direct LOS links rely upon a direct path between the transmitter and receiver, while diffuse systems generally rely upon light reflections from walls, ceilings and other diffuse reflecting surfaces. Direct LOS links provide high power efficiency and minimize multipath dispersion, but can suffer from shadowing. Diffuse systems provide robustness against signal blockage and shadowing, enabling mobile users to instantly connect and collaborate in a wireless environment. However, they are more prone to multipath dispersion, which causes pulse spread and intersymbol interference (ISI), in addition to poor power efficiency and much-reduced data rate compared to direct LOS links. Furthermore, transmitter beam diversity was proposed as a method that can be implemented to enhance the performance of optical wireless (OW) communication systems [3]–[6]. A multibeam transmitter is used to create multiple diffusing spots that point in different directions towards reflecting surfaces. A simple structure of diffusing spots in a line strip multibeam system (LSMS) was examined in [6] and shown to produce SNR improvement compared to a conventional diffuse system (CDS) or a uniform multibeam system. However, mobility and shadowing can induce significant SNR performance degradation in OW systems [7]. Various techniques have been proposed to combat the limitations of OW systems, and higher bit rates have been achieved [8]–[14]. OW links offer the opportunity for high-speed communications as well as the potential to achieve data rates well beyond 10 Gbit/s with full mobility, although these have not been demonstrated to date. Up to 12.5 Gbit/s OW data transmission with limited mobility has been successfully demonstrated through experiments [15]. Although significant research has been done, much more work is needed before even a fraction of the potential bandwidth is achieved in practical systems. The research presented in this study aims to address the impairments of OW systems and provide practical solutions, hence achieving data rates beyond those reported in [8]–[15], but more importantly it focuses on speeding up the adaptation process associated with these adaptive systems. This paper reports systems that offer OW channel bandwidths of more than 15 GHz, which enables the OW system to support operations at data rates beyond 15 Gbit/s. The improvements achieved are based on channel and noise modeling and not on actual measurements. However, the results obtained have been compared to published simulation and experimental work (simpler systems:

Manuscript received May 15, 2013; revised September 30, 2013; accepted October 13, 2013. Date of publication November 4, 2013; date of current version November 11, 2013. This work was supported by the Deanship of Scientific Research (DSR), King Abdulaziz University, Jeddah, under Grant Gr/33/9.

F. E. Alsaadi is with the Department of Electrical and Computer Engineering, King Abdulaziz University, Jeddah, Saudi Arabia (e-mail: fuad_alsaadi@yahoo.com).

M. A. Alhartomi is with the School of Electronic and Electrical Engineering, University of Leeds, Leeds LS2 9JT, U.K. (e-mail: elmal@leeds.ac.uk).

J. M. H. Elmirghani is with the Department of Electrical and Computer Engineering, King Abdulaziz University, Jeddah, Saudi Arabia. He is also with the School of Electronic and Electrical Engineering, University of Leeds, Leeds LS2 9JT, U.K. (e-mail: j.m.h.elmirghani@leeds.ac.uk).

Digital Object Identifier 10.1109/JLT.2013.2286743

CDS [4] and spot diffusing with angle diversity receivers [5]) to validate the simulator and calculation methods and good agreement was observed, giving confidence in the simulator when examining other systems. For example [4] predicts CDS bandwidth of 37 MHz, here we predict 38 MHz, see Section IV-A. Furthermore, [5] predicts almost 2 GHz channel bandwidth for spot-diffusing with 7° diversity receivers, and here we predict 1.82 GHz and 2.1 GHz, respectively, for diversity spot-diffusing with 8° FOV and 4° FOV.

Beam angle and power adaptation has been shown to be an effective method that can help optimize the spot distribution and the power among the spots so as to maximize the receiver's SNR, regardless of the transmitter position [8]. Significant SNR and bandwidth improvements were achieved, combined with complexity expansion in terms of the computation time required to optimize the receiver's SNR. In this study, we aim to speed up the angle adaptation algorithm, and aim to achieve much more power efficiency compared to the original multibeam angle adaptive system (MBAAS). The fast angle adaptation algorithm introduced converges towards the optimum spot distribution through efficient use of a divide and conquer algorithm. It works by recursively breaking down the scanning process into a number of iterations with different scan rates (see Section III-A). In an initial previous work [9] we have introduced the concept of fast adaptation through a divide and conquer approach. Here we extend the work in [9] by (i) reshaping the spot distribution (including consideration of both the optimum number of spots and the pattern associated with how these spots are distributed), (ii) considering the algorithm complexity, (iii) considering a real environment that experiences shadowing, and (iv) evaluating high data rate system (15 Gbit/s). In [10] Alresheedi and Elmirghani have designed holograms using simulated annealing to generate multibeam spots and in order to reduce the number of holograms to be generated and speed-up the search for the best hologram from the finite hologram vocabulary they have used a divide and conquer algorithm similar to that in [9] and examined the impact of having a finite hologram vocabulary on SNR and delay spread.

Channel dispersion associated with multipath propagation is an important concern in designing indoor OW systems. Multipath dispersion causes the received pulse to spread, resulting in ISI. An angle diversity receiver employing uncorrelated narrow FOV detectors oriented in different directions can be beneficially used to reduce the impact of multipath propagation due to the limited range of rays captured [5]–[9]. However, it has to be noted that in spot-diffusing OW systems, the delay spread is dictated by the number of spots seen within the receiver's FOV and their relative positions. Therefore switching on the beams at the same time may induce a time delay between the signals received from the spots within the receiver FOV, which results in spreading the received pulse and hence limiting the bandwidth. The signal spread observed by the receiver can be compensated for by introducing a differential time delay between the beams at the transmitter through beam delay adaptation. In effect, the multibeam transmitter adaptively switches on the beams in a fashion that allows all the signals to reach the receiver at the same time. This can help the system reduce multipath dispersion and ISI at higher bit rates. The beam delay adaptation technique was proposed in [11] and it is used here as it is shown to offer improvements in terms of bandwidth efficiency.

In this paper, a fast and efficient angle adaptation (FEAA) algorithm is introduced to the OW diversity spot-diffusing system design to spatially optimize the spot distribution (the number and pattern of spots) with the aim of maximizing the receiver SNR, as well as significantly reducing the computation time required. This fast and efficient adaptation algorithm is then followed by a beam delay adaptation method to reduce multipath dispersion, hence minimizing the delay spread at the receiver. To further improve the quality of the link, we also employ beam power adaptation. The link design proposed here has the ability to alter the number of spots, the pattern (or position of spots), the beam delays and beam powers so as to optimize the SNR and delay spread at a given receiver location. A liquid crystal (LC) device can be used to adaptively vary the direction and intensity of the beams and their switching times at relatively low complexity [16], [17]. The adaptation requires training and feedback from the receiver to the transmitter, and a low data rate diffuse channel is suggested to achieve this feedback. The main goal is to reduce the effect of transmitter/receiver mobility and the associated impacts on SNR and bandwidth. The effectiveness of the link design in the presence of shadowing and signal blockage is also studied.

The next section gives a description of the OW system model. The receiver structure is given in Section III. Section IV describes the fast and efficient adaptation algorithms. The performance of the mobile multibeam adaptive OW system and the simulation results are outlined in Section V. System complexity and adaptation time are considered in Section VI. The robustness of the proposed link design against shadowing and signal blockage is investigated in Section VII. Section VIII introduces high-speed indoor OW communication systems. Finally, conclusions are drawn in Section IX.

II. OW System Model

A. Simulation Environment

The characteristics of a mobile channel formed by a fast and efficient adaptive multibeam transmitter, coupled with an angle diversity receiver, are investigated. Simulation was conducted in an empty room with floor dimensions of 8 m × 4 m (length × width), and ceiling height of 3 m. Experimental measurements have shown that most building materials including plaster walls (with the exception of glass) are approximately Lambertian reflectors [1]. In this study, it is assumed that all reflecting surfaces in the set-up room are Lambertian reflectors with high reflectivity (reflection coefficient of 0.8 for walls and ceiling, 0.3 for floor). High reflectivity was chosen as it results in the highest multipath dispersion (worst case), and thus significant pulse spread. Reflections from doors and windows are considered to be the same as reflections from walls. To model the reflections, the room reflecting surfaces were divided into a number of equal-size, square-shaped reflection elements with area dA and reflection coefficient ρ. These elements act as secondary emitters and were modeled as Lambertian reflectors.

It was found through previous investigations that third-order reflections and higher produce a weak contribution to the received optical power [1]–[4]. Reflections up to second-order are therefore considered in this study. The impulse response in a practical OW system is continuous; however, the simulator subdivides the reflecting surfaces into discrete elements. The effect of discretization can be reduced by subdividing time into bins of widths Δt and grouping the powers received within each bin into a single received power. This accounts for the smoothness seen in the resulting impulse responses presented in this paper. A good choice for the bin width is $\Delta t = \sqrt{dA}/c$, which is roughly the time light takes to travel between neighboring elements. An identical histogram to the actual impulse response is achieved as dA approaches zero. It should be noted that reducing dA leads to improved resolution in impulse response evaluation, together with an increase in the computation time. To keep the computation within reasonable time and measure, a surface element size of 5 cm $\times$ 5 cm is used. The corresponding time period (bin width) used in computations is 0.17 ns. A smaller time bin (0.01 ns duration) was also used with the proposed multibeam adaptive OW systems, resulting in a slightly higher delay spread compared to that obtained using the 0.17 ns time bin. Reflecting elements of 0.3 cm $\times$ 0.3 cm were used in the case of a time bin of 0.01 ns. Note that at very small delay spread levels a time bin with a smaller duration has to be used. This reduces the smoothing effect introduced through the use of time bins (that group rays with comparable delays together).

To quantify the proposed system's performance under mobility, three new multibeam transmitter configurations are considered: a fast and efficient angle adaptive system (FEAAS); a fast and efficient angle and delay adaptive system (FEADAS); and a fast and efficient angle, delay and power adaptive system (FEADPAS), in conjunction with an angle diversity receiver of seven branches. Comparisons of the traditional LSMS and the original MBAAS are also considered. All the proposed systems use an upright transmitter with 1 W optical power, and the transmitter is placed at three different locations on the CF: (2 m, 4 m, 1 m), (1 m, 1 m, 1 m) and (2 m, 7 m, 1 m). These transmitter locations represent three main cases: transmitter at centre of room, transmitter at room corner, and transmitter near walls. Computer-generated holographic beamsplitters are assumed to be mounted on the emitter to shape its output to multiple narrow beams, which in turn form a line of diffusing spots on the ceiling (LSMS configuration). The optimum spot distribution, which yields the best receiver SNR in the original MBAAS, can be chosen following the original angle adaptation algorithm given in [8]. The new FEAAS (which is discussed in Section IV-A) can guide the multibeam transmitter to optimize its spot distribution (the number and more so the pattern of the spots) so as to maximize the receiver's SNR with a higher power efficiency and much reduced search time, compared to the original MBAAS. The delays and power levels associated with the beams can be adjusted according to the procedure discussed in Sections IV-B and IV-C. An array source and a LC holographic element can generate the beams. Changing the holographic 2D function (through an LC device) can generate variable optical spot locations (on the ceiling and/or walls) with different optical spot intensities and differential switching times. The delay adaptation can be implemented through array element delayed switching. Most of the adaptive holographic switches are LC based [16], [17]. These devices have microsecond response times [16], [17] which are adequate, given that the adaptation process has to be carried out at the rate at which the environment changes (for example, human motion) and not at the data rate. However, the design of such holograms and their implementation through LC devices is not ideal, where the input power may not be all assigned to spots and may partially leak through [3], [18]. For example, it is shown in [18] that the design of a hologram that diffuses the laser may result in a hot spot with a large peak power, reducing the efficiency of the power distribution and hologram design. Similarly, in the design of a multibeam pattern here, some power may leak through or all the power may not be assigned to spots thus reducing the efficiency. This may result in a form of noise where beams are not directed at the correct spatial orientations desired. The effect of such noise (a form of background noise) is of interest in the overall design, but is not considered here. The effect of noise due to signal leakage (where data is not directed at the correct spatial orientations desired (spots)) is however much lower compared to BN as the signal power is much lower than the BN power. Furthermore in Section VI, we investigate the performance penalty associated with having spots in spatial locations other than the correct ones. It has to be noted that the spatial spot locations misalignment errors in Section VI associated with mobility in the absence of continuous adaptation are much larger than the spatial errors associated with imperfect hologram design (the ones discussed here). The adaptation requires training and feedback from the receiver to the transmitter, and a low data rate diffuse channel is suggested to achieve this feedback. At a low data rate the angle, delay and power associated with such a beam can be maintained at a fixed level.

B. Channel Characteristics and Ambient Light Modeling

In OW communication links, intensity modulation with direct detection (IM/DD) is the preferred choice. Multipath propagation in an indoor OW channel using IM/DD can be characterized by the impulse response $h(t)$ of the channel [3]

$$I(t) = R\ \ x(t) \otimes h(t) + n(t), \tag{1}$$

where $I(t)$ is the received instantaneous current at the output of the photodetector at a certain position, t is the absolute time, $x(t)$ is the transmitted instantaneous optical power, $\otimes$ denotes convolution, R is the photodetector responsivity, and $n(t)$ is the BN, which is modeled as white and Gaussian, and independent of the received signal. The dominant source of noise in indoor optical wireless systems is artificial ambient light such as, incandescent lamps and fluorescent lamps. These sources emit a substantial amount of power within the wavelength range of silicon photodetectors introducing shot noise, and can saturate the photodetector when their intensity is high [19]. Although ambient light can be much stronger than the transmitted data signal, certain measures (such as optical filters) can be used

to minimize its influence [20]. Despite the use of such a filter, the background shot noise current produced by incandescent lights is much higher in level than that produced by low- and high-frequency fluorescent lights [21]. No optical filters have been used in this study. In order to assess the system performance in a realistic situation, the link was exposed to directive noise sources, eight halogen spotlights, which cause high optical spectral corruption levels to the received data stream. The Philips PAR 38 Economic was chosen and this emits a power of 65 W in Lambertian beams with $n_{\mathrm{beam}} = 33.1$, where n_{beam} is the mode number of the radiation beam that describes the beam shape, where the higher the n_{beam} the narrower the light beam. The eight spotlights were placed 2 m above the communication floor (CF), which is a surface 1 m above the floor, at (1, 1, 3), (1, 3, 3), (1, 5, 3), (1, 7, 3), (3, 1, 3), (3, 3, 3), (3, 5, 3), and (3, 7, 3). Interference from daylight through windows and doors was not considered in this study. Furthermore, in order to minimize the BN effect and reduce multipath dispersion, a diversity receiver is implemented.

III. Angle Diversity Receiver

In contrast to the single wide FOV receiver, an angle diversity receiver is a collection of narrow-FOV detectors oriented in different directions. The receiver's diversity system considered consists of seven photodetector branches, each with a responsivity of 0.54 A/W. The direction of each photodetector is defined by two angles: azimuth (Az) and elevation (El) angles. The El angles of six photodetectors remained at 70°, while the seventh one was given an El of 90°. The Az angles were fixed at 0°, 0°, 45°, 90°, 180°, 225°, and 270°. The azimuth (Az) angle is the orientation angle of the photodetector with respect to the *x-axis*. Therefore, the detector oriented along the *x-axis* has Az angle of 0° (i.e., Az = 0°). The detector facing up has a conical field of view and therefore it is azimuth agnostic, i.e., can be assumed to have any values of Az, however for mathematical convenience we chose its azimuth angle as Az = 0°. The Az, El, and FOVs were chosen through an optimization similar to that in [6]. Moreover, the angle diversity receiver was designed so that all the photodetectors always point to the ceiling. This choice of the receiver characteristics (Az, El and FOVs) produces a link that is robust against diffusing spot blockage, as well as preventing shadowing due to moving objects. This can also help the multibeam fast and efficient angle adaptive transmitter to cluster its diffusing spots on the ceiling, where the diversity receiver can spatially select the photodetector that observes high power and minimum background noise. This can result in maximizing the SNR at the receiver. Each photodetector is assumed to employ a compound-parabolic concentrator (CPC), which has an acceptance semi-angle ψ_C so that when the reception angle δ exceeds ψ_C, the concentrator transmission factor, $T_C(\delta)$, rapidly approaches zero. The CPC is a common non-imaging concentrator and has $\psi_C < 90°$, a refractive index of $N_C = 1.7$ is considered, and the entrance area is $A = 9\pi/4$ cm^2. The CPC's transmission factor is given by [22]

$$T_{c,NIMG}(\delta) = T[1 + (\delta/\psi_C)^{2H}]^{-1}, \tag{2}$$

where $T = 0.9$ and $H = 13$ [23]. The CPC has an exit area of $A' = A\sin^2(\psi_C)/N_C^2$.

The diversity receiver is always placed on the CF along the $x = 1$ m or $x = 2$ m lines. Each photodetector employs a CPC with an acceptance semi-angle of $\psi_C = 8°$, and is assumed to be fitted exactly into its associated concentrator's exit area. The photosensitive area of each photodetector is therefore 4.7 mm^2. Furthermore, in order to use small area detectors at the high data rates considered, the corresponding concentrator's acceptance semi-angle of each photodetector is restricted to 4°, resulting in a reduction in the detector area to 1 mm^2. The size of the concentrator is acceptable in mobile terminals and this can be ruggedly fixed to the photodetector. The photocurrents received in the various detectors are amplified separately, and the resulting electrical signals are processed in an approach that maximizes the power efficiency of the system. Several possible diversity schemes, such as select-best (SB), equal gain combining (EGC), and maximum ratio combining (MRC) can be considered. For simplicity, SB is considered here in order to process the resulting electrical signals. SB represents a simple form of diversity, where the receiver simply selects the branch with the best SNR. In order to compute the impulse response on the entire CF, a simulation package based on a ray-tracing algorithm [6], [7] was developed for arbitrary transmitter-receiver configurations in an arbitrary room size that has diffuse reflectors. Diversity of emissions and detection were taken into account. Additional features were introduced to enable beam angles, delays and powers to be adapted. The received multipath profiles due to each spot were computed at each photodetector, based on the detector's FOV and the area the detector observes at each set of transmitter and receiver locations. The resultant power profile at each photodetector is the sum of the powers due to the total number of diffusing spots considered. Several parameters are of interest and can be derived from the simulated impulse response, such as:

1) root-mean-square delay spread (D), which measures the temporal dispersion of the received signal due to multipath propagation [6]

$$D = \sqrt{\frac{\sum_{m=1}^{M_{\mathrm{rays}}} (t_m - \mu)^2 P_m^2(t_m)}{\sum_{m=1}^{M_{\mathrm{rays}}} P_m^2(t_m)}},\quad \mu = \frac{\sum_{m=1}^{M_{\mathrm{rays}}} t_m P_m^2(t_m)}{\sum_{m=1}^{M_{\mathrm{rays}}} P_m^2(t_m)} \tag{3}$$

where t_m is the time delay associated with the m^{th} ray received with a power of $P_m(t)$, M_{rays} is the total number of rays captured and μ is the mean delay.

2) 3-dB channel bandwidth, which is equal to the frequency at which the magnitude response decreases by 3 dB.

IV. Transmitter Configurations

In this section, three new adaptive multibeam transmitter configurations are presented, analyzed, and compared in order to identify the most suitable geometry for use in indoor OW systems. LSMS is one of the attractive configurations in the literature, therefore it is modeled and used for comparison purposes in order to evaluate the improvements offered through the proposed novel configurations. LSMS uses a diffusing spot distribution

pattern where a line of spots with equal intensities (in this case 80 spots) is formed in the middle of the ceiling, i.e., at $x = 2$ m and along the *y-axis* when the transmitter is placed at the centre of the room. The difference in distance between adjacent spots is 10 cm. These spots become secondary emitters which emit Lambertian radiation. The positions of the spots are dictated by the transmitter location. As the transmitter moves, the distribution of the spots can be determined in the room following the procedure given in [7]. Furthermore, the new adaptive configurations (FEAAS, FEADAS, and FEADPAS) are introduced and evaluated next.

A. FEAAS

Beam angle adaptation (beam steering based on LC devices) was shown to be an efficient technique that can identify the optimum spot distribution, hence providing a strong path between the diffusing spots and the receiver, regardless of the transmitter position [8]. An optical transmitter, followed by an adaptive hologram was used to generate variable optical spot locations based on the alteration of the transmission angles (θ_x and θ_y) between -90° and 90° in the $x-y$ axes with respect to the transmitter's normal. Essentially the adaptive hologram was made to initially produce a single spot, which is then scanned along a number of possible positions (on the ceiling and walls) to identify the optimum location that yields the best SNR at the receiver. The adaptation algorithm changes the beam transmission angles (θ_x and θ_y) between -90° and 90° in the $x-y$ axes with respect to the transmitter's normal. An LC device can be used for beam angle adaptation and can help achieve the wide angle steering proposed here [17]. The implementation choices and their optimization warrant further study and are beyond the scope of this paper. The beam in each step forms a diffusing spot centered at coordinates of (x_s, y_s, z_s) within the room (in the ceiling or walls). The beam angles θ_x and θ_y (spherical coordinates) and spot location (x_s, y_s, z_s) (Cartesian coordinates) are related to the transmitter location (x_T, y_T, z_T) and the room dimensions (length $\times$ width $\times$ height) as shown in Table I. The position of the spot (i.e., the corresponding coordinates) that yields the best SNR at the receiver is chosen as the optimum location. Note that the coordinate system refers to the centre of the spot. Note that in this new system (FEAAS), we recursively break down the scanning process into a number of iterations that focus recursively into smaller regions in space resulting in different scan step sizes (i.e., each scan iteration uses a different angle adaptation step size). The new system makes efficient use of a divide and conquer algorithm that breaks down a problem into a number of related sub-problems, these becoming eventually simple enough to be solved directly. Accordingly, the new fast and efficient adaptation algorithm divides the entire room into four arbitrary quadrants and selects the quadrant that includes the sub-optimum location (best SNR among the four quadrants) as a new scan area. The next scan iteration is then started within the selected quadrant, using half of the previous scan step size with the aim of identifying a new sub-optimum location. Similarly, the selected quadrant is divided into four arbitrary sub-quadrants, and the sub-quadrant including the new sub-optimum location is chosen as a new scan area for the next iteration. This process is repeated for a number of iterations where the number of iterations chosen depends on the acceptable complexity and acceptable SNR penalty, both will be discussed in Sections V and VI.

TABLE I
SPHERICAL COORDINATES TO CARTESIAN COORDINATES CONVERSION ALGORITHM

Algorithm I: Spherical Coordinates to Cartesian Coordinates Conversion		
1	L = 800 cm;	(length of the room)
2	W = 400 cm;	(width of the room)
3	H = 300;	(height of the room)
4	z_{CF} = 100 cm;	(height of the CF)
5	Identify the Cartesian coordinates (x_s, y_s, z_s) of a spot formed by a beam with transmission angles θ_x and θ_y (Spherical Coordinates) at a transmitter location of (x_T, y_T, z_T) as follows:	
6	Initially calculate the x-coordinate as: $x_s = x_T - (H - z_{CF})tan(\theta_x)$	
7	Initially calculate the y-coordinate as: $y_s = y_T - (H - z_{CF})tan(\theta_y)$	
8	if $x_s > W$	(the spot is in the West y-z Wall)
9	$x_s = W$; and	$z_s = ((x_T - x_s)/tan(\theta_x)) + z_{CF}$;
10	Elseif $x_s < 0$	(the spot is in the East y-z Wall)
11	$x_s = 0$; and	$z_s = ((x_T - x_s)/tan(\theta_x)) + z_{CF}$;
12	Elseif $y_s > L$	(the spot is in the South x-z Wall)
13	$y_s = L$; and	$z_s = \left((y_T - y_s)/tan(\theta_y)\right) + z_{CF}$;
14	Elseif $y_s > L$	(the spot is in the North x-z Wall)
15	$y_s = 0$; and	$z_s = \left((y_T - y_s)/tan(\theta_y)\right) + z_{CF}$;
16	Else	
17	$z_s = H$;	
18	End	

For fair theoretical comparison purposes, the iterations can continue until a certain angle adaptation step size is reached, i.e. until reaching the angle step size used in the original MBAAS for example, where the optimum spot location with the best receiver SNR is identified. Furthermore, once the optimum beam direction is identified, a set of uniformly distributed spots (25×25 spots are considered here), at 1 cm apart, initially created and centered at the optimum location. The receiver's SNR due to each spot is computed separately and relayed to the transmitter at a low data rate. The transmitter then determines which one of the possible 25×25 spot locations house an illuminated spot based on a threshold, where the spots that produce SNRs higher than the threshold are illuminated, whilst the others are disregarded. The threshold is based on the received SNR achieved at the receiver through a diffuse transmitter with a transmitted power that is identical to the spot power (in this case the transmitter is assumed to produce 25×25 spots and each spot is assigned 1.6 mW). This can guarantee that only the spots having direct contributions at the receiver (i.e., the spots located within the receiver's FOV) will be illuminated. A depiction of the FEAAS configuration is shown in Fig. 1. For a single transmitter and a single receiver at a given set of positions, the

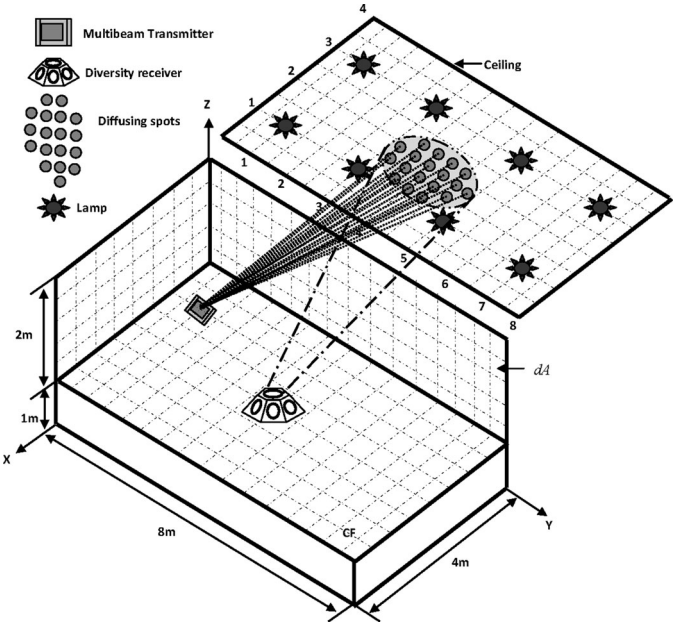

Fig. 1. OW FEAAS architecture at transmitter and receiver locations of (1 m, 1 m, 1 m) and (2 m, 4 m, 1 m), respectively.

FEAAS identifies the optimum beam direction and shapes the optimum spot distribution, according to the following steps:

1) Configure the adaptive hologram to implement the first scan iteration according to its associated parameters: the angle adaptation step size (θ_{steps}), the *x-axis* scan range (θ_x^{start} to θ_x^{end}) and the *y-axis* scan range (θ_y^{start} to θ_y^{end}). In order to initially scan the entire room, the x-y axes scan ranges are set to -90° and 90°. Furthermore, the θ_{steps} is initially set to 17.74°, allowing the spot to move 64 cm in each step, and resulting in a total of 160 possible locations in the entire room.
2) Produce a single spot and move it by varying the beam angles: θ_x and θ_y in steps of θ_{steps} along the x-y axes. The beam angle θ_x is changed between θ_x^{start} and θ_x^{end}, while θ_y is varied between θ_y^{start} and θ_y^{end}.
3) Compute the receiver SNR at each step and send a feedback signal at a low rate to inform the transmitter of the SNR associated with the step.
4) At the step where the receiver SNR is maximum, record the associated transmission angles θ_x^{subopt} and θ_y^{subopt}.
5) Reconfigure the adaptive hologram to implement the next iteration as follows:
   a) Reset the angle adaptation step size as $\theta_{\text{steps}} = \theta_{\text{steps}}/2$.
   b) If $\left|\theta_x^{\text{subopt}}\right| \leq \left(\left|\theta_x^{\text{end}}\right| - \left|\theta_x^{\text{start}}\right|\right)/2$, then reset the higher scan range along the *x-axis* as $\theta_x^{\text{end}} = \theta_x^{\text{subopt}}$ and keep the lower scan range as it is. Otherwise, reset the lower scan range along the *x-axis* as $\theta_x^{\text{start}} = \theta_x^{\text{subopt}}$ and keep the higher scan range as it is.
   c) If $\left|\theta_y^{\text{subopt}}\right| \leq \left(\left|\theta_y^{\text{end}}\right| - \left|\theta_y^{\text{start}}\right|\right)/2$, then reset the higher scan range along the *y-axis* as $\theta_y^{\text{end}} = \theta_y^{\text{subopt}}$ and keep the lower scan range as it is. Otherwise, reset the lower scan range along the *y-axis* as $\theta_y^{\text{start}} = \theta_y^{\text{subopt}}$ and keep the higher scan range as it is.
6) Repeat steps 2 to 5 for a number of iterations (four scan iterations are considered).
7) Stop when the minimum allowed angle adaptation step size is reached (i.e., a certain scan step size of 2.29° that is used in the original MBAAS). In the FEAA algorithm, four iterations are carried out where the first scan iteration uses a step size of 17.74° and the fourth (and final) one is set to a 2.29° scan step size. In effect, the fast "divide and conquer" algorithm has to scan 640 possible locations to identify the optimum spot location. This results in a new angle adaptive system that is almost 20 times faster than the original MBAAS, where 12500 locations had to be scanned.
8) Determine the $x_{\text{opt}}, y_{\text{opt}}$, and z_{opt} position of the spot that maximized the receiver's SNR. This $(x_{\text{opt}}, y_{\text{opt}}, z_{\text{opt}})$ coordinate can be defined based on the optimum transmission angles θ_x^{opt} and θ_y^{opt}.
9) Generate a set of uniformly distributed spots (25×25 spots in this case), at 1 cm apart, whose centre is this coordinate, i.e., $(x_{\text{opt}}, y_{\text{opt}}, z_{\text{opt}})$.
10) Equally distribute the total power, 1 W, among the spots, compute the power received at the diversity receiver, and calculate the SNR.
11) Select the best link (the photodetector with the best SNR) to use as a desired communication link (desired photodetector), in essence the diversity receiver implements "select best" combining.
12) Individually turn on each spot, compute the power received at the desired photodetector, as well as calculate the SNR.
13) Inform the transmitter of the SNR associated with the spot by sending a feedback signal at a low rate.
14) Repeat steps 12 and 13 for all the spots.
15) Optimize the number and shape of the spots by illuminating the spots that produce SNRs higher than a threshold value and omitting the others. As mentioned earlier, this threshold value is set in proportion to the SNR produced by a diffuse transmitter.
16) Operate the multibeam transmitter with the optimum spot distribution (the optimum number of spots and optimum pattern) while the beams propagate with equal intensity at the same time.

It should be noted that the adaptation algorithm described above applies to the single user case, i.e., a single transmitter and a single receiver position. The medium access control (MAC) protocol should include a repetitive training period that allows the adaptation steps to be performed. Training should be carried out at the rate at which the environment changes. This is usually a slow rate, commensurate with human motion. Pedestrians move typically at a speed of 1 m/sec [24]. Furthermore, the new multibeam adaptive OW system (FEAAS) is more robust against changes in the receiver's orientation compared to the original MBAAS. This is due to the ability of the FEAA algorithm to optimize the spot distribution (including the number

and shape of the diffusing spots) so as to maximize the receiver SNR, regardless of the transmitter position and the receiver orientation.

B. FEADAS

The transmitted signal propagates to the receiver through various paths of different lengths. Therefore, switching ON the beams at the same time may result in receiving the signals at different times due to multipath propagation. This may spread the received pulse and cause ISI. However, if the switching times of the beams can be adjusted to allow the beam with the longest journey to travel first and then the other beams with differential delays, all the rays can reach the receiver at the same time. This can be achieved through beam delay adaptation. The transmitter and receiver are synchronized and, at the start of a frame, the transmitter individually switches on the spots, each after a predetermined time interval T. The receiver observes the deviation (differential delay) associated with the arrival of pulses compared to the issuing time rhythm of T seconds. The received multipath profile (impulse response) due to each spot is observed at the receiver, and its mean delay (time delay) is then calculated with respect to the start of the frame. In effect, the receiver receives the first pulse at time (t_1), the second pulse at time $T + t_2$ and the last pulse at time $\left((N_{\text{spot}} - 1)\, T + t_{N_{\text{spot}}}\right)$, where N_{spot} is the total number of diffusing spots considered. The time delay $(t_i, i = 1, 2, ..., N_{\text{spot}})$ attributed to the varying path length associated with each spot can then be determined. For example, the differential delay between the first pulse (spot) and second pulse (spot) attributed to their varying channel path lengths is $|t_2 - t_1|$. The varying response times of the individual receivers may add a jitter element to this value if their response is slow or if they are not implemented on a common integrated platform; the latter may reduce variability. The time delays associated with the beams are relayed to the transmitter to help optimize the delay spread at the receiver. In effect, the multibeam transmitter switches on the beams at different times, starting with the beam that induces the maximum time delay. The other beams sequentially propagate to the receiver, each at a certain time that is proportional to the difference between its associated time delay and the maximum time delay. In contrast to the previous configuration (FEAAS), where the multibeam transmitter radiates all the beams at the same time, in this system the beams are switched on at different times, with the aim of minimizing the delay spread at the receiver. In both systems (FEAAS and FEADAS) the transmitted power is equally distributed among the beams. Once the optimum spot distribution is identified, the new delay adaptation algorithm adjusts the switching times of the beams as follows:

1) It switches on each spot individually, computes the power received at the desired photodetector, as well as calculating the mean delay (time delay).
2) It sends a feedback signal at a low rate to inform the transmitter of the mean delay associated with the beam (spot).
3) It repeats steps 1 and 2 for all the spots.
4) It sets the beam with the maximum mean delay as a first traveler and introduces a time delay to the switching time of each of the rest of the beams in proportion to the difference between its associated mean delay and the maximum mean delay.
5) It configures the multibeam transmitter to operate with the optimum spot distribution, optimum beam delays, and with the power equally distributed among the beams.

Note that if a spot is switched on and no pulse is received due to signal blockage, this spot will be disregarded and the total power will be distributed among the unobstructed beams. The time delays associated with unobstructed beams will be determined and relayed to the transmitter to help optimize the delay spread at the receiver.

At the transmitting end, if discrete or array sources are used to implement the transmitter, then electronic control can be used to facilitate switching ON these sources with nanosecond delays, which is implementable in electronics. If a hologram is used to generate the beams in a spatial light modulator, then stored frames corresponding to different spot outputs can be loaded. LC devices are readily able to modulate the beam within tens or hundredths of microseconds, although nanosecond response times have been demonstrated [16]. Having identified the delays, the transmitter coupled with a set of discrete sources can switch on the beams with the required delays using electronic control. The use of fewer sources can simplify the transmitter. The penalty induced in link performance will be small, though this warrants further study.

C. FEADPAS

In contrast to the previous multibeam adaptive OW system (FEADAS), where the total power, 1 W, is equally distributed among the beams, in this system (FEADPAS) the total power is distributed unequally so as to further optimize the SNR and delay spread at the receiver. In effect, the spot nearest to the receiver is allocated the highest power level, whilst the farthest spot is assigned the lowest power level, so as to further maximize the SNR and bandwidth at the receiver. This transmitter identifies the optimum number of beams and their directions (beam angles), introduces a time delay between the beams and adjusts the power distribution among the beams in a fashion that optimizes the SNR and delay spread at the receiver. This can be achieved through the algorithm given in Table II. This algorithm applies to the single user case where the spot distribution, beam delays and beam powers are adapted so as to maximize the SNR and bandwidth at one given receiver location. In a multi-user scenario, opportunistic scheduling [25] can be employed where the optimum spot distribution (optimum number and pattern of the diffusing spots), beam delays and beam powers are chosen to maximize the SNR and bandwidth in a given region (i.e., set of users) for a given time period.

The proposed system is designed to interconnect mobile communication devices placed on the CF. If one (or more) of these devices is fixed and is connected to a backbone network, it can act as an access gateway to the external world and can also act as a base station that shares the resources among the mobile

TABLE II
FAST AND EFFICIENT ANGLE, DELAY, AND POWER ADAPTATION ALGORITHM

Algorithm II: Fast and Efficient Angel, Delay and Power Adaptation

$N_{spot} = 25 \times 25$; (number of spots)

$N_{photodetector} = 7$; (number of photodetectors)

$p(\cdot)$ is a rectangular pulse defined over $[0, T_b]$, where $T_b = 1/B$ (B is a bit rate)

$\theta_x^{start} = -90^o$ and $\theta_x^{end} = 90^o$ (the lower and higher scan ranges along the x-axis)

$\theta_y^{start} = -90^o$ and $\theta_y^{end} = 90^o$ (the lower and higher scan ranges along the y-axis)

$\theta_{steps} = 17.74^o$ (the angle adaptation step size, which is 17.74^o for the first iteration)

$N_{iteration} = 4$;(number of scan iterations considered)

For $k = 1 : N_{iteration}$

  For $i = \theta_x^{start} : \theta_{steps} : \theta_x^{end}$

    For $j = \theta_y^{start} : \theta_{steps} : \theta_y^{end}$

      $\theta_x = i$; $\theta_y = j$; (transmission angles in the x-y axes)

      Produce a single spot in a direction associated with θ_x and θ_y based on the Spherical Coordinates to Cartesian Coordinates conversion algorithm given in Table I

      For $l = 1 : N_{photodetector}$

        Calculate and sum the received powers within a time bin (0.01 ns duration)

        Produce the impulse response $h_l(t)$

        Calculate the pulse response as $h_l(t) \otimes p(t - T_b)$ and then, find $(P_{s1} - P_{s0})_l$

        Compute

$$SNR_l = \left(R \times (P_{s1} - P_{s0})_l \Big/ (\sigma_t)_l \right)^2$$

      End

      $SNR(i,j) = max(SNR_l)$;

      $detector(i,j) = find\big(SNR_l == max(SNR_l)\big)$;

    End

  End

$SNR_{max} = max\big(SNR(i,j)\big)$;

$\left[\theta_x^{subopt}, \theta_x^{subopt}\right] = find(SNR(i,j) == SNR_{max})$; (identify the suboptimum location)

$bestlink = detector\big(\theta_x^{subopt}, \theta_x^{subopt}\big)$; (select the desired photodetector)

If $\left|\theta_x^{subopt}\right| \le \left(\left|\theta_x^{end}\right| - \left|\theta_x^{start}\right|\right)/2$ (reset the new scan range in the x-axis)

$\theta_x^{end} = \theta_x^{subopt}$;

Else

$\theta_x^{start} = \theta_x^{subopt}$;

End

If $\left|\theta_y^{subopt}\right| \le \left(\left|\theta_y^{end}\right| - \left|\theta_y^{start}\right|\right)/2$ (reset the new scan range in the y-axis)

$\theta_y^{end} = \theta_y^{subopt}$;

Else

$\theta_y^{start} = \theta_y^{subopt}$;

End

$\theta_{steps} = \theta_{steps}/2$; (reset the new scan step size)

End

$\theta_x^{optimum} = \theta_x^{subopt}$; $\theta_y^{optimum} = \theta_y^{subopt}$; (identify the optimum spot direction)

Generate a uniformly distributed spots (25×25) centered by a location associated with $\theta_x^{optimum}$ and $\theta_y^{optimum}$

For $s = 1 : N_{spot}$

  $P_s = 1/N_{spot}$; (the power per spot)

  Compute the impulse response observed by the desired photodetector

  Calculate $\mu_s = \sum_m t_m P_r^2(t_m) \Big/ \sum_m P_r^2(t_m)$; (mean delay due to spot s)

  Calculate

$$W_s = SNR_s = \left(R \times (P_{s1} - P_{s0})_s \Big/ (\sigma_t)_s \right)^2 ;$$

(spot's weight)

End

$W_{max} = max(W_s)$; $\mu_{max} = max(\mu_s)$;

$P_{limit} = 0.001$; (1mW is the eye safe limit at the near infrared wavelengths)

$W_{thr} = SNR_{CDS}$; (threshold proportional to the SNR produced by a diffuse transmitter)

$W_s(W_s < W_{thr}) = 0$; (set the spot's weight that is lower than the threshold to zero)

$W_{total} = sum(W_s)$; (total of spots' weights)

For $s = 1 : N_{spot}$

  $P_s = W_s/W_{total}$; (distribute the power among the spots in proportion to their SNRs)

  $P_s = (W_s/W_{max}) \times P_{limit}$; (introduce a restriction so that the spot power does not exceed $1mW$)

  $\Delta t_s = \mu_{max} - \mu_s$; (calculate the time delay)

  Compute the impulse response $h_s(t)$ observed by the desired photodetector

  Shift the impulse response as $h_s(t - \Delta t_s)$ (introduce the time delay)

End

Sum the delayed impulse responses within a time bin (0.01 ns duration)

Produce the optimized impulse response $h_{optimized}(t)$ due to all the spots considered

Calculate the pulse response = $h_{optimized}(t) \otimes p(t - T_b)$ and then, find $(P_{s1} - P_{s0})$

Compute $SNR_{optimized} = \left(R \times (P_{s1} - P_{s0}) \Big/ \sigma_t\right)^2$;

Compute

$$D_{optimized} = \sqrt{\sum_m (t_m - \mu)^2 P_r^2(t_m) \Big/ \sum_m P_r^2(t_m)},$$

where, $\mu = \sum_m t_m P_r^2(t_m) \Big/ \sum_m P_r^2(t_m)$

devices and coordinates access to the medium. The design of a suitable medium access control protocol for such a system is not considered here and is worth further investigation. In addition, the employment of opportunistic scheduling techniques can enable simultaneous transmission of a video content from a source to a set of destinations (users). Such content distribution networks can make use of BitTorrent or peer-to-peer protocols [26] which suit the OW environment, the latter is inherently peer-to-peer in nature. The adaptation takes place at a rate comparable to the rate at which the environment changes and/or the rate of transmitter and receiver motion. This is typically a low pedestrian rate in indoor OW systems, which relaxes the demands placed on the feedback channel, the computation circuits and the LC device and ensures that the associated MAC overheads are minimal. The absolute optimality of this algorithm is worth further investigation, we show here the level of improvement it offers.

V. Performance Analysis and Simulation Results

The performance of the proposed multibeam adaptive algorithms (FEAAS, FEADAS and FEADPAS in conjunction with diversity reception) is evaluated in the presence of ambient light noise, multipath propagation and mobility. Comparisons with the LSMS and the original MBAAS are also presented.

A. OW Channel Characteristics

The channel impulse response specifies the received optical power resulting from multipath propagation. The impulse responses of the proposed multibeam OW configurations are depicted in Fig. 2. The impulse response of a CDS is included. It should be noted that the value of the received power reported in this section is the peak level of the pulse response that was obtained through convolution of the impulse response with a rectangular transmitted pulse of 1 W and 20 ns duration, corresponding to 50 Mbit/s bit rate. Furthermore, the delay spread values reported throughout the paper are the root-mean-square (rms) delay spread (D) values, which measure the temporal dispersion of the received signal due to multipath propagation, given by (3). It is clearly seen that the spot-diffusing structure is significantly better than the CDS when both systems employ a wide FOV receiver [see Fig. 2(a)]. This is due to the presence of direct path components between the diffusing spots and the receiver, made possible through spot-diffusing geometry. CDS produces 1.56 μW received optical powers with much more signal delay, an rms delay spread of almost 2.65 ns (over a long time period) corresponding to a channel bandwidth of 38 MHz, due to the diffuse transmission and wide receiver FOV (FOV $=$ 90°). A significant increase in the received power from 1.56 μW (CDS) to 3.07 μW can be achieved when an LSMS replaces the CDS, and when both systems employ a wide FOV receiver. This significant increase in the received power comes with a reduction in the signal spread (delay spread) from 2.65 ns to 0.92 ns. The delay spread of the LSMS signal can be reduced from 0.92 ns to 0.21 ns when a 25° diversity receiver is employed instead of the wide FOV receiver. However, a reduction in the received optical power from 3.07 μW to 1.67 μW is induced. This is due

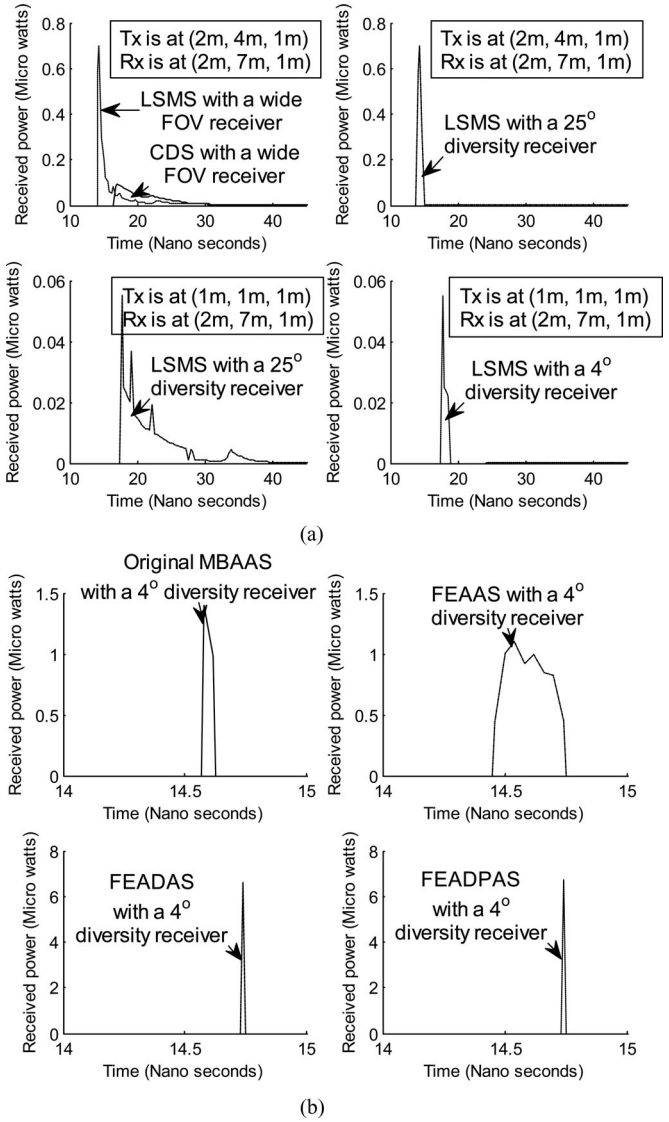

Fig. 2. Impulse responses of different OW configurations: (a) CDS and LSMS with a wide FOV receiver, and LSMS with a 25° and 4° FOV diversity receivers, and (b) the original MBAAS, FEAAS, FEADAS, and FEADPAS with a 4° FOV diversity receiver, at two transmitter positions: (1 m, 1 m, 1 m) and (2 m, 4 m, 1 m), and when the receiver is located at (2 m, 7 m, 1 m).

to the limited range of rays captured by narrow FOV diversity receivers. Nonetheless, it has to be observed that LSMS, with an angle diversity receiver offers a better overall SNR than LSMS with a wide FOV receiver, due to the significant reduction in the collected BN [6]. Transmitter mobility increases the delay spread of the diversity LSMS, as might be expected, at receiver locations away from the transmitter. For example, when the receiver is located at (2 m, 7 m, 1 m) and the transmitter moves from the centre of the room to the corner (1 m, 1 m, 1 m), the delay spread of the 25° diversity LSMS increases from 0.21 ns to 4.1 ns. This transmitter movement can also cause an increase in the path loss, where the collected optical power drops from 1.67 μW to 0.6 μW. Limiting the FOV of the diversity receiver to 4° reduces the delay spread from 4.1 ns to almost 0.31 ns, and decreases the received power from 0.6 μW to 0.13 μW, due

TABLE III
3 dB CHANNEL BANDWIDTH OF THE PROPOSED MULTIBEAM SYSTEMS

Configuration	3 dB Channel Bandwidth (GHz)						
	Receiver locations along the y-axis, Y (m)						
	1	2	3	4	5	6	7
LSMS	2.1	1.6	1.2	0.89	0.77	0.67	0.56
Original MBAAS	8.3	8.7	8.3	8.7	8.3	8.7	8.3
FEAAS	2.8	3.2	2.8	3.2	2.8	3.2	2.8
FEADAS	15.2	15.4	15.2	15.4	15.2	15.4	15.2
FEADPAS	15.5	15.6	15.5	15.6	15.5	15.6	15.5

to the limited range of rays captured. A reduction in the delay spread from 0.31 ns to 0.019 ns can be achieved if the spot distribution is spatially adjusted to positions near the receiver through beam angle adaptation (i.e., when the MBAAS is employed instead of the traditional LSMS). This improvement in the delay spread comes with an increase in the received optical power from 0.13 μW to 2.4 μW. Furthermore, an improvement in the received optical power, from 2.4 μW to 6.6 μW, can be achieved when an FEAAS replaces the original MBAAS. This is attributed to the ability of the new FEAAS to fully benefit from the transmitted power through optimizing the number and more so the pattern of the spots, based on the receiver's location and its FOV, and equally distributing the transmitted power among the spots. This improvement in the received power is achieved while accelerating the adaptation process by a factor of 20 compared to the search time required in the original MBAAS. However, an increase in the delay spread from 0.019 ns to 0.073 ns is incurred due to the increase in the number of rays captured by the receiver (as a result of increasing the number of spots, where 25 $\times$ 25 spots are employed instead of a line of 80 spots). The received signal spread can be dramatically reduced from 0.073 ns to 0.011 ns through adjusting the switching times of the beams so that all the rays reach the receiver at the same time, thus reducing the effect of multipath dispersion. Although a reduction in the delay spread is achieved when an FEADAS replaces the FEAAS, the received power is similar in both systems. This is due to the similarity of the spot geometry and power distribution in both systems. However, the FEADAS adapts the switching times of the beam to allow the rays to be captured by the receiver at the same time. It has to be observed that FEADAS offers a better overall SNR compared to FEAAS at high bit rates due to the significant reduction in the ISI (see Fig. 7). To further improve the quality of the link, we combine these new techniques (fast beam angle and delay adaptation with the new 25 $\times$ 25 spot geometry) with beam power adaptation. The results achieved through this combination are better than previous results in this area. In addition, the impulse responses for all the cases studied are analyzed to compare the impact of transmitter/receiver mobility on the received optical power, and to examine the extent to which the combination of the proposed methods ameliorate this effect. The results are presented in terms of channel bandwidth and SNR. The 3 dB channel bandwidth of the proposed multibeam OW systems (LSMS, original MBAAS, FEAAS, FEADAS and FEADPAS with a 4° diversity receiver) is given in Table III. The results show that FEADPAS

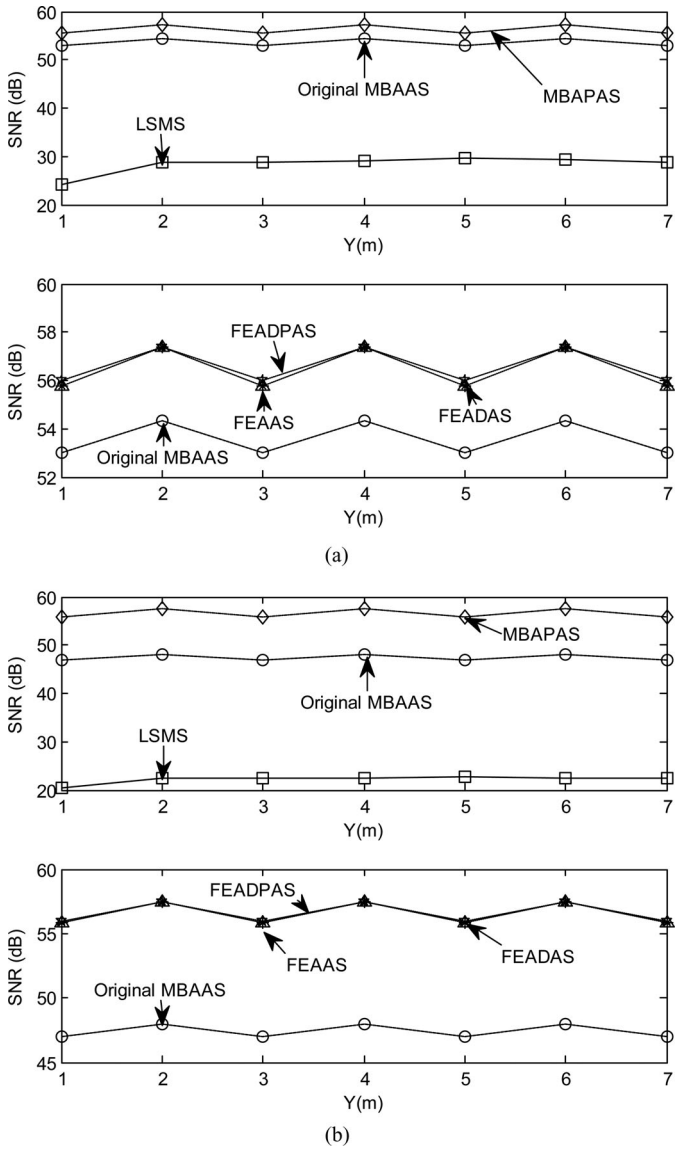

Fig. 3. SNR of the proposed systems, in conjunction with (a) an 8° diversity receiver and (b) a 4° diversity receiver, when the transmitter is at (2 m, 7 m, 1 m) and the receiver moves along the $x = 1$ m.

can offer OW communication channels with 3 dB bandwidths greater than 15 GHz. In addition, the number of spots visible within the receiver FOV is a key factor to achieve acceptable SNR (greater than 15.6 dB for a bit error rate (BER) of 10^{-9}). Due to this fact, the FEAAS can improve the SNR by increasing the number of diffusing spots visible within the receiver's FOV, particularly when using narrower FOVs (see Fig. 3). This can allow the FEAAS transmitter to transmit lower optical power, while meeting the SNR requirements and conforming to eye safety regulations. However, it has to be noted that, the delay spread is dictated by the number of spots seen within the FOV and their relative positions. This can result in introducing a time delay between the signals received from the spots within the receiver's FOV, and hence limiting the bandwidth. The increase in the number of rays captured by the receiver in the FEAAS as a result of increasing the number of spots, 25 $\times$ 25 spots

are employed here instead of employing a line of 80 spots in the original MBAAS, results in a higher delay spread as well as a lower bandwidth, compared to the original MBAAS, see Table III.

B. SNR Analysis

Indoor mobile OW communication systems are strongly impaired by the shot noise induced by ambient light noise. The probability of error (P_e) in an indoor mobile OW communication system is given by

$$P_e = Q\left(\sqrt{\mathrm{SNR}}\right) \tag{4}$$

where $Q(x) = (1/\sqrt{2\pi})\int_x^\infty e^{-(x/\sqrt{2})^2}\,dz$ is the Gaussian function, which assumes a value of 6 for a probability of error $P_e = 10^{-9}$, an SNR of 15.6 dB. Considering the impact of pulse spread caused by ISI where $P_{s1} - P_{s0}$ accounts for the eye opening at the sampling instant, the SNR is given by [6]

$$\mathrm{SNR} = \left(\frac{R \times (P_{s1} - P_{s0})}{\sigma_t}\right)^2 \tag{5}$$

where P_{s0} and P_{s1} are the powers associated with logic 0 and 1 respectively. The total noise variance σ_t^2 is made up of three components: (i) the noise associated with the preamplifier component σ_{pr}^2 (which is a function of the receiver topology adopted, i.e., thermal noise), (ii) the background light-induced shot noise σ_{bn}^2 and (iii) the shot noise components σ_{s0}^2 and σ_{s1}^2 associated with P_{s0} and P_{s1}, respectively. This signal-dependent noise, σ_{si}^2, is very small (in non-optically pre-amplified systems) and can be neglected. The noises σ_0^2 and σ_1^2 associated with logic 0 and 1 respectively are given as

$$\sigma_0^2 = \sigma_{pr}^2 + \sigma_{bn}^2 + \sigma_{s0}^2 \text{ and } \sigma_1^2 = \sigma_{pr}^2 + \sigma_{bn}^2 + \sigma_{s1}^2. \tag{6}$$

Substituting (6) in (5) with $\sigma_t = \sigma_0 + \sigma_1$ [27], the SNR is given by

$$\mathrm{SNR} = \left(\frac{R \times (P_{s1} - P_{s0})}{\sqrt{\sigma_{pr}^2 + \sigma_{bn}^2 + \sigma_{s0}^2} + \sqrt{\sigma_{pr}^2 + \sigma_{bn}^2 + \sigma_{s1}^2}}\right)^2. \tag{7}$$

To enable comparison with previous work [7], a bit rate of 50 Mbit/s was used. A higher bit rate of 15 Gbit/s was also considered for the proposed multibeam adaptive OW systems. The preamplifier used in the 50 Mbit/s OW system (20 ns pulse duration) is the 70 MHz PIN-BJT design proposed by Elmirghani *et al*. [28], with noise spectral density of 2.7 $pA/\sqrt{Hz}$. This receiver introduces little or no distortion onto the 50 Mbit/s pulse stream. The performance of the proposed multibeam adaptive OW systems (FEAAS, FEADAS and FEADPAS), coupled with an angle diversity receiver, is evaluated under the constraints of ambient light noise, multipath propagation and mobility. The systems' SNRs are also compared to those of the LSMS and the original MBAAS with diversity detection, when the transmitter is placed at (2 m, 7 m, 1 m) and the receiver moves along the $x = 1$ m line. These locations were selected in order to examine some of the key cases, i.e., points exactly underneath directive noise sources, as in $y = 1$ m, 3 m, 5 m, and 7 m, as well as points near the corner of the room, which represent the worst communication paths, as well as central and other room locations along the $x = 1$ m line that represent normal operation. Note that the $x = 3$ m line is similar to the $x = 1$ m line due to symmetry in the room and the $x = 2$ m line is a better line as it is away from noise sources. We have therefore examined a worst case scenario. The results are shown in Fig. 3, where all OW systems operate at 50 Mbit/s. Previous work [7] showed that the LSMS SNR, with a diversity receiver, is largely independent of the receiver's location when the transmitter is stationary at the centre of the room as a result of the good spot distribution on the ceiling. It was also found that degradation in the LSMS SNR is observed when the transmitter is mobile, due to having some non-illuminated regions in the room and having some others with an increased spot population. Regardless of the transmitter position, beam angle adaptation can help the multibeam transmitter to cluster its diffusing spots (a line of 80 spots) at an area on the ceiling and/or walls based on the receiver location so as to maximize the receiver SNR [8]. The results in Fig. 3(a) show that a significant SNR improvement of 29 dB can be achieved when MBAAS replaces LSMS at a 6 m transmitter-receiver distance, when both systems employ an 8° diversity receiver. This is in good agreement with the results reported in [8]. The MBAAS identifies the optimum location through an exhaustive ordinary search and then distributes the spots in the form of a line strip with equal intensities. This may lead to power being allocated to some spots outside the receiver FOV hence wasting some of the transmitted power, particularly when using narrower FOVs. The use of narrower FOVs is essential in some cases to reduce noise and interference, and also to allow the use of smaller area detectors. The results in Fig. 3 also show that a power penalty of 6 dB can be induced in the original MBAAS SNR when a 4° diversity receiver replaces the 8° diversity receiver. This power penalty can be compensated for with an SNR improvement of approximately 9 dB if the power is adaptively distributed among the spots through beam power adaptation, i.e., when the multibeam angle and power adaptive system (MBAPAS) replaces the original MBAAS. MBAPAS was proposed and examined in [8], and here it is modeled and used for comparison purposes. However, power adaptation will not help much in this case if the power per spot is restricted due to eye safety. Increasing the number of spots in the line strip is possible, but also will not help here as the number of spots located within the receiver FOV is limited.

Therefore optimizing the number and, more so, the pattern of the spots is an important design consideration. The proposed system (FEAAS) can reduce the adaptation time through the use of a divide and conquer algorithm, and can also optimize the number and pattern of the spots based on the receiver FOV. This can help the receiver collect more power, while helping with eye safety regulations. In addition, Fig. 3(b) shows that the new FEAAS offers an improvement in the SNR of 9 dB over the original MBAAS. This SNR improvement comes with a reduction in the computation cost in the practical OW FEAAS by making use of a divide and conquer algorithm. The proposed system (FEAAS) therefore outperforms the original MBAAS in terms of both SNR and adaptation speed. Although additional

bandwidth efficiency is achieved through beam delay adaptation (i.e., when an FEADAS is employed) compared to the FEAAS, a comparable SNR is seen in both systems at 50 Mbit/s bit rate. This is due to the excess channel bandwidth achieved by the FEAAS (OW channel bandwidth of 2.8 GHz) which guarantees that ISI does not occur at the lower bit rate considered (50 Mbit/s). However ISI can cause significant degradation in the SNR at higher bit rates. Despite this, replacing the FEAAS by an FEADPAS, at a bit rate of 50 Mbit/s, can slightly improve the SNR, by less than 0.5 dB. Note that the new FEAAS in this case is able to achieve the majority of the improvement through optimizing the number and more so the pattern of spots based on the receiver's location and the receiver's FOV, and equally distributing the power among the spots. If shadowing exists (i.e., some beams are obstructed), then the new FEAAS can re-optimize the spot distribution (including the number of spots and the shape of their distribution) so that the transmitted power is equally distributed only to unobstructed beams. The SNR in (5) accounts for the impact of ambient light noise and preamplifier noise, and therefore the SNR values reported reflect both impairments. The BN effect is manifested here as a fluctuation in the SNR of the adaptive multibeam OW systems. This is due to the BN having a very low value at $y = 2$ m, 4 m, and 6 m, as the receiver is not underneath a spotlight, while high noise levels are detected at $y = 1$ m, 3 m, 5 m, and 7 m. In effect, when the receiver is underneath a spotlight the adaptive multibeam transmitter is not able to distribute its diffusing spots within the FOV of the detector facing up, and instead it clusters the spots within one of the side detector's FOV.

VI. System Complexity and Adaptation Time

Significant SNR improvements can be achieved through the use of the proposed adaptation algorithms, however the implementation complexity increases. This complexity is associated with the computational time and resources required to identify the optimum spot position where the receiver's SNR at each possible beam location is computed and the optimum spot direction is selected at the transmitter. This complexity also results from computing the SNR and time delay due to each beam at the receiver and adapting the power levels and time delays among the spots at the transmitter. The transmitter computations are simple and the receiver operations are comparable to those needed when implementing receiver diversity, and as such the complexity increase is moderate. However, we aim here to evaluate the efficiency of our algorithms through the study of both time complexity and memory size criteria. The computational complexity can be measured based on the nature of the function $T(n)$ [29], where for instance a linear algorithm of input size n can induce a linear time complexity of $T(n) = O(n)$. An algorithm with complexity order $O(n)$ usually has a single pass implementation and shows acceptable performance with small n, however it becomes too complex with larger n. The classical angle adaptation algorithm can identify the optimum location through scanning all the possible locations, which are processed in the basic "one-pass" style. Therefore, the time complexity of this algorithm is linear given by $T(n) = O(n)$ and its complexity rises with increase in n. The input size n here represents the total number of possible beam locations that have to be scanned to identify the optimum beam location that results in the best SNR. In contrast, the fast algorithm is a recursive algorithm based on a "divide and conquer" approach, where the scanning process is recursively broken down into a number of iterations k. Four iterations are conducted in our case (i.e., $k = 4$), where $n/64$ locations have to be scanned in each iteration, resulting in a time complexity given as [29]

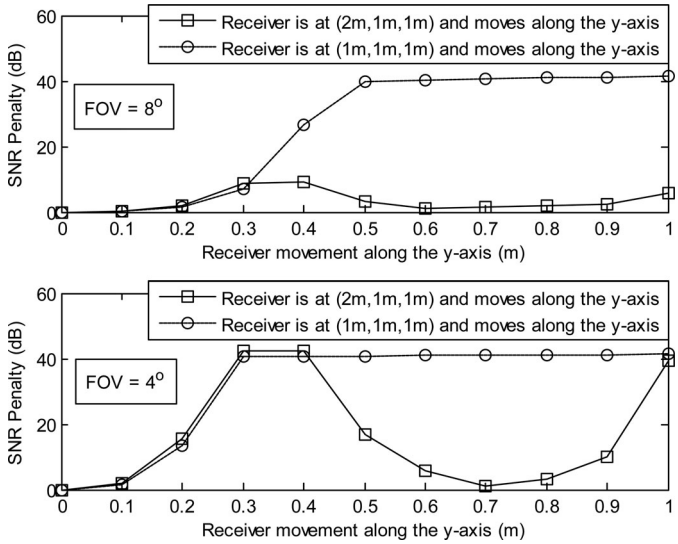

Fig. 4. SNR penalties of the proposed system (FEADPAS) when the receiver moves by a distance of 1 m away from the optimum location of the spots.

$$T(n) = k\,T\left(\frac{n}{64}\right) + kj = kT\left(\frac{n}{j\,(2^k)}\right) + kj$$
$$= \log\left(\frac{n}{j}\right) T(1) + j\log\left(\frac{n}{j}\right) = j\log\left(\frac{n}{j}\right) \quad (8)$$

where j is the number of subproblems (quadrants in our case). In each iteration the fast algorithm divides the scanning area into four quadrants (i.e., $j = 4$). Accordingly, the fast algorithm can achieve time optimal $O(4\log_2(n/4))$ complexity, and therefore it is highly efficient compared to the classical algorithm. It should also be noted that, the fast algorithm needs a memory space of 64 times lower than that used in the classical algorithm.

To reduce the computational complexity, the system may choose to update its beam angles, power and delay less frequently even in the presence of mobility. This simplification is at the cost of an SNR penalty. We studied the SNR penalty based on the transmitter using its old adaptation settings, i.e., old beam angles, old beam delays and old beam powers, while in motion. This is to determine how often the system has to adapt its settings based on a link margin. The SNR penalties incurred as a result of mobility (distance moved along the *y-axis*) and non-adaptation of weights are depicted in Fig. 4, when two different diversity receivers (8° FOV diversity receiver and 4° FOV diversity receiver) are used. Two main cases exist and are shown. Firstly when the receiver is under a spotlight and secondly when

the receiver is away from a spotlight; and we consider receiver motion by 1 m along the *y-axis*.

The SNR penalty was calculated for each receiver movement in step of 10 cm. When an 8° FOV diversity receiver moves by a distance of 20 cm away from the optimum location of the spots at (2 m, 1 m, 1 m) and no adaptation is carried out, the SNR of the proposed system (FEADPAS) degrades by 1.8 dB. Higher SNR penalties of 8.9 dB and 9.3 dB can be incurred if the 8° FOV diversity receiver moves further by 10 cm and 20 cm respectively. However, if the receiver continues moving the SNR penalty reduces until it reaches a value of almost 1 dB at a receiver location away from the optimum location of the spots by 70 cm. This is due to the fact that when the receiver is located at (2 m, 1 m, 1 m) (i.e., it is not underneath a spotlight) the transmitter can steer its beams to positions within the FOV of the detector facing up. Once the receiver starts moving (while no further adaptation is carried out) some of the spots will move out of the FOV of the detector facing up and start to appear within the FOV of the side detectors. With more movement steps the spots start to appear outside the FOV of the side detectors and the SNR penalty increases accordingly. In contrast, when the receiver is located at (1 m, 1 m, 1 m) (i.e., underneath a spotlight) the transmitter is not able to allocate its spots within the FOV of the detector facing up and instead clusters the spots within the view of one of the side detectors. When the receiver moves away from the optimum location of the spots, some of the spots move outside the receiver FOV thus incurring a power penalty, as a result of using the old adaptation settings. This power penalty increases with increase in the distance away from the optimum location and saturates at a value of 40 dB approximately after a movement of 50 cm. This is attributed to the fact that beyond this transmitter-receiver distance all the spots fall outside the receiver FOV, and the achieved SNR is due to reflections only (i.e., no LOS is established). The case where a 4° FOV diversity receiver is used can be similarly explained. It should be noted that the adaptation process can be done in milliseconds based on typical LC device characteristics. This is fast enough given that the adaptation has to track the channel variation which happens at the rate at which humans or indoor objects move. However, the system design can allow an SNR margin (for example, 3 dB) to ensure that the adaptation process does not have to be repeated frequently. The new fast "divide and conquer" algorithm needs to scan 640 locations to identify the optimum spot location. Once the optimum beam direction is identified, a set of uniformly distributed spots (25×25 spots) at 1 cm spacing is created and centered at the optimum location. The receiver's SNR (due to each spot) is estimated separately and relayed to the transmitter to help shape the optimum spot distribution. If each SNR computation/estimation is carried out in 10 μs [16], then the total adaptation time when the receiver moves to a new location is almost 13 ms. When an 8° FOV diversity receiver is used we considered all the typical representative set of transmitter and receiver locations (transmitter at centre of room, transmitter at room corners etc, receiver moves along the $x = 1$ m, $x = 2$ m, near walls and near corners etc.) and the worst penalty identified when the transmitter or receiver moves by 20 cm and no adaptation is carried out was almost 2 dB. Therefore, with a 1 m/s pedestrian movement/environmental change, there is at least 0.2 s interval between one adaptation and the next. It is suggested that the receiver re-evaluates its SNR every 0.2 s and relays this to the transmitter, which in turn initiates a new adaptation if the receiver's SNR has significantly changed (compared to a threshold). As such, the holograms can adapt every 0.2 s, and the 13 ms adaptation time therefore represents a spot reconfiguration overhead time of approximately 6.5%. Holograms based on LC devices capable of adapting within ms times are feasible. It should be noted that the adaptation process has been done at the rate at which the environment changes and not at the system's bit rate. Therefore, the proposed system (FEADPAS) can achieve 15 Gbit/s when it is stationary, and 93.5% of this data rate, i.e., 14 Gbit/s when there are environmental changes (see Fig. 7). Following a similar approach in the case of a 4° FOV diversity receiver, adaptation has to be done if the transmitter or receiver moves by 0.1 m or more if an SNR penalty lower than 3 dB is desired. The penalty in this case associated with 0.1 m motion is 1.7 dB. The adaptation process needs therefore to be repeated every 0.1 s, representing an overhead of 13% in terms of transmission time, and as such the system can achieve 13 Gbit/s when it is on the move. The 4° FOV diversity receiver is used here to allow the use of small area detectors at these high data rates. The link budget can be further improved if imaging receivers with MRC are used, and this warrants further study. It should also be noted that if the receiver chooses the spot with the best SNR and reports this value (spot index) to the transmitter to allocate all the available power to this spot, the complexity will be reduced. However, such a system will be prone to beam blockage, shadowing and may violate eye safety. The proposed system offers advantages in this regard; however there is a moderate increase in receiver complexity, as discussed above.

VII. Robustness to Shadowing and Signal Blockage

The effectiveness of the FEAAS is evaluated in a harsh environment with mobility. Such an environment is typically encountered in real office configurations, where optical signal blockage owing to cubicles, windows, doors and furniture exists. Furthermore, other impairments also degrade the system in this real environment including ambient light noise, and multipath propagation. To simulate shadowing and signal blockage of the communication links, the room shown in Fig. 5 is considered. This room represents a realistic office environment, and its dimensions are similar to those of the room previously considered. The glass windows are assumed not to reflect any signal. The reflectivity of the ceiling and walls surrounding the windows is 0.8. Two perpendicular walls are covered with bookshelves and filing cabinets with a 0.4 reflectivity. Cubical office partitions are assumed to either absorb or block signals. The complicated environment in this room results in shadowing created by physical partitions and low reflectivity objects. Comparisons were carried out between the traditional LSMS, adaptive LSMS (ALSMS) and FEAAS when all systems employ a 4° diversity receiver and operate at 50 Mbit/s in a complicated room design

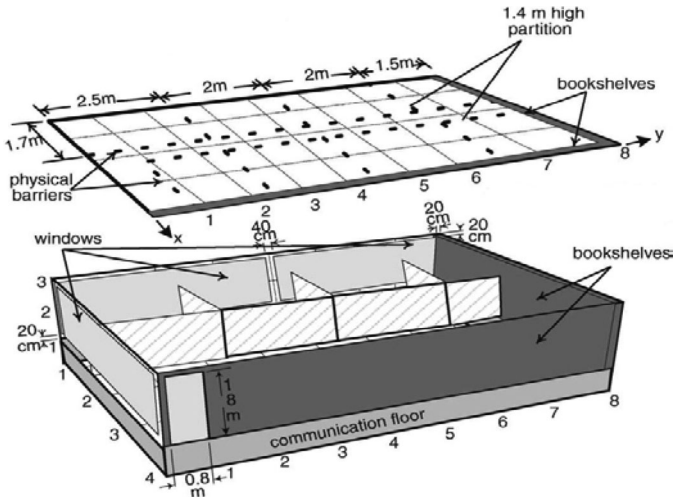

Fig. 5. A realistic office that has three large glass windows, a door, a number of rectangular-shaped cubicles with surfaces parallel to the room walls, and other furniture such as bookshelves and filing cabinets.

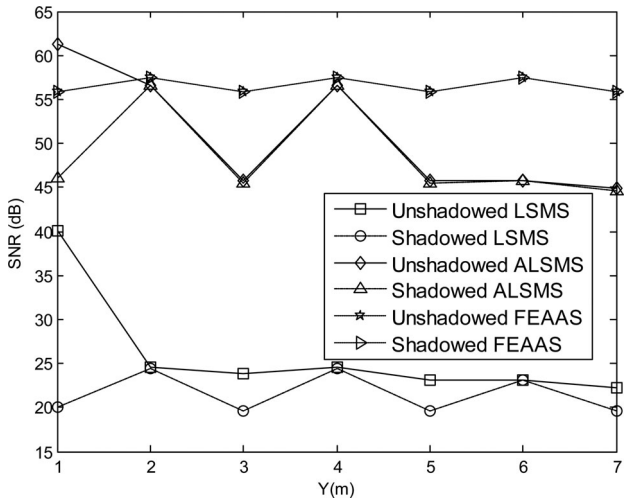

Fig. 6. SNR of three multibeam OW systems: LSMS, ALSMS, and MBFPE-AAS with a 4° diversity receiver in two room scenarios (unshadowed and shadowed) when the transmitter is placed at (1 m, 1 m, 1 m) and the receiver moves along the $x = 1$ m line.

with full mobility. The arrangement in the ALSMS is similar to that in LSMS, but the power is adaptively distributed among the spots in the ALSMS, with the aim of maximizing the receiver's SNR. The SNR results of the proposed systems in two room scenarios (shadowed and unshadowed rooms) are depicted in Fig. 6, when the transmitter is placed at (1 m, 1 m, 1 m) and the receiver moves along the $x = 1$ m line on the CF. The complicated environment shown in Fig. 5 represents a shadowed room, while the unshadowed one is that referred to as the empty room described in Section II. It is to be noted that this line ($x = 1$ m) represents the worst zone that can be scanned due to the presence of office cubicles. The worst impact of shadowing and signal blockage in the LSMS performance translates to an SNR degradation of almost 20 dB when the transmitter and receiver are co-located in the corner of the room (1 m, 1 m, 1 m). This degradation is due to the presence of windows that cause a large signal loss and hence larger path losses near the corner of the room. Furthermore, the effect of signal obstruction due to partitions can be observed as a degradation in the SNR level by approximately 4 dB when the receiver is located at $y = 3$ m, 5 m and 7 m. At these locations ($y = 3$ m, 5 m and 7 m) the diversity receiver is underneath a spotlight and in turn it relies on one of the side photodetectors in order to achieve its best SNR, in essence "select best" combining is implemented. The receiver proximity to partitions in these cases may cause path blockage to some of the direct rays (depending on the receiver directionality and the height of partitions) resulting in performance penalties. In contrast, shadowing and signal blockage have almost no or limited effect on the LSMS SNR at locations of $y = 2$, 4 and 6 m where the receiver is not underneath a spotlight. When the transmitter is placed in the corner of the room (1 m, 1 m, 1 m) and the diversity receiver is located at (1 m, 2 m, 1 m) or (1 m, 4 m, 1 m), the results indicate that among the photodetectors considered, the one facing up is able to collect the maximum power possible (through a number of diffusing spots located within its FOV) and with minimum noise level. This can help the receiver achieve a similar SNR at these sets of transmitter and receiver locations, in the two room scenarios (shadowed and unshadowed rooms), as shown in Fig. 6. However, shadowing can reduce the reflection contribution. This reduction is very low due to the employment of narrow FOVs (FOV $= 4°$), and therefore it does not affect the overall SNR since the photodetector facing up is still able to see the same number of spots, even in the presence of shadowing. The comparable LSMS SNR observed in both shadowed and unshadowed environments at transmitter and receiver locations of (1 m, 1 m, 1 m) and (1 m, 6 m, 1 m) can be similarly explained, though the side photodetector having an El and Az of 40° and 270° respectively is the best link selected in this scenario. Furthermore, ALSMS with a 4° diversity receiver is more robust against shadowing and signal blockage compared to LSMS, owing to its ability to re-allocate power to unblocked spots. These benefits are manifest as a comparable SNR performance in the 4° diversity ALSMS system in both shadowed and unshadowed rooms, except in the scenario where the transmitter and receiver are co-located in the corner of the room (1 m, 1 m, 1 m). In this case, shadowing and signal blockage can induce a degradation of 15 dB in the ALSMS SNR. This is due to the inability of the beam power adaptation to assign higher powers to the spots located on the side wall near the receiver due to the presence of windows, and instead the transmitted power is allocated to the ceiling spots. This penalty can be put in context by observing that an SNR improvement of almost 26 dB can be achieved when the ALSMS replaces the traditional LSMS in a shadowed environment when both systems employ a 4° diversity receiver and operate at 50 Mbit/s. This SNR improvement illustrates the gain achieved through power adaptation while the beam angles are kept fixed. Previous work [8] showed that further SNR improvement of 10 dB can be achieved if adaptation is also applied to beam angles, i.e., if an MBAPAS replaces the ALSMS. Here we show that a multibeam OW system adopting the new FEAAS can provide a robust link against shadowing and signal blockage, and can also achieve an SNR performance comparable to that obtained by MBAPAS. This is achieved

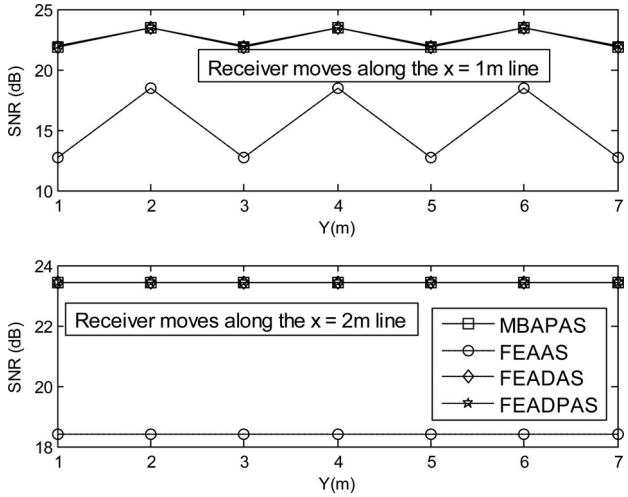

Fig. 7. SNR of the multibeam systems (MBAPAS, FEAAS, FEADAS, and FEADPAS) operating at 15 Gbit/s when the 4° diversity receiver moves along the $x = 1$ m and $x = 2$ m lines within a shadowed environment.

together with a reduction in the system adaptation complexity by a factor of 20, while distributing the transmitted power among the spots in equal intensities (i.e., power adaptation is not employed in this system). This achievement is attributed to the ability of the new system (FEAAS) to adapt to such environments and shape the optimum spot distribution by illuminating the unblocked spots only, hence maximizing the receiver's SNR. Beam delay adaptation can help increase the channel bandwidth, thus improving the SNR when the system operates at higher bit rates, due to the reduction in the effect of multipath dispersion and ISI (see Fig. 7). The results obtained and presented in Fig. 6 prove that the 25 cm $\times$ 25 cm array is quite enough to combat shadowing and beam blockage in a realistic environment such as that in Fig. 5. Furthermore, spreading the beams more widely will result in higher dispersion and not necessarily improve the performance under blockage any more than the proposed 25 cm $\times$ 25 cm array, which is shown to perform well. In addition, two main cases exist when ALSMS and FEAAS are compared. These two cases refer to a receiver under a spotlight or away from a spotlight. In Fig. 6, the transmitter is at (1 m, 1 m, 1 m) and therefore when the receiver is at (1 m, 2 m, 1 m) and (1 m, 4 m, 1 m), the ALSMS is able to use its detector facing up as these positions are not under spotlights. Therefore, ALSMS and FEAAS perform similarly. At (1 m, 3 m, 1 m), (1 m, 5 m, 1 m) and (1 m, 7 m, 1 m) the receiver is under spotlights and as such the FEAAS outperforms ALSMS as it is able through angle adaptation to move its beams and locate them within the FOV of side detectors that do not observe any background noise. At (1 m, 6 m, 1 m) although the receiver is not under a spotlight, yet the ALSMS is not able to beam steer and hence its spots are at the far (1 m, 1 m, 1 m) corner and are shadowed and unseen by the receiver. This is also partly the case at (1 m, 5 m, 1 m) and fully the case at (1 m, 7 m, 1 m).

VIII. High-Speed Mobile Indoor OW Communication Systems

The high SNR achieved through the multibeam fast power, angle and delay adaptation algorithm, coupled with the additional bandwidth shown in Table I, can be used to provide higher data rates (15 Gbit/s and beyond). The PIN-HEMT design proposed by Kimber *et al*. [30] was used for the proposed 15 Gbit/s multibeam adaptive OW systems. This preamplifier has a noise current spectral density of 11 $pA/\sqrt{Hz}$ and a bandwidth of 12 GHz. The preamplifier bandwidth can be limited to 10.6 GHz through the use of appropriate filters. The optimum receiver bandwidth is 0.707 $\times$ bit rate (Personick's analysis [31]). The modulation format used is on-off keying (OOK) with intensity modulation and direct detection. The rise and fall times of laser diodes, transmitter and receiver design are not considered in this paper as transceivers for data rates up to 10 Gbit/s are well established in fibre systems [32], [33]. The particular features of OW transceiver design here are of interest in future work. Note that narrow FOV receivers, which use small detectors compatible with fibre systems receivers, are employed here. In previous work, we considered holographic spot diffusing transmitters [8]. OOK is the simplest modulation scheme to implement in OW systems, and is therefore used here. OOK is an appropriate modulation scheme for high bit rate OW systems [34] due to its simplicity and the ability of laser diodes to switch on and off at rates into Gbit/s. However, ISI can be significantly increased. Although ISI can be effectively reduced by utilizing an equalization technique [35] this is not used here. Furthermore, it should be noted that the SNR calculations reported take into account the eye closure (see (5), where $P_{s1} - P_{s0}$ caters for eye closure), and therefore the SNR values reported reflect ISI as well as receiver preamplifier noise and BN impairments. The simulation results, depicted in Fig. 3, indicate that the two systems (FEAAS and FEADAS) can perform identically at a bit rate of 50 Mbit/s, and this is evident in the excess channel bandwidths achieved, which guarantees that ISI does not occur at the lower bit rate considered (50 Mbit/s). However, ISI can increase significantly if the FEAAS operates at 15 Gbit/s, and hence significant SNR degradations can be induced. In contrast, the FEADAS can offer a bandwidth of more than 15 GHz (see Table I), which enables it to support operation at 15 Gbit/s, at least. Fig. 7 shows that a considerable SNR improvement of 9 dB can be achieved when an FEADAS replaces the FEAAS, and where both systems employ a 4° diversity receiver with a reception area of 1 mm^2 and operate at 15 Gbit/s at 6 m transmitter-receiver distance in a shadowed environment. Note that the transmitted power is equally distributed among the beams in both systems (FEAAS and FEADAS), and this improvement is due to the significant reduction in the influence of multipath dispersion and ISI through beam delay adaptation. The SNR can be slightly improved further by approximately 0.2 dB if the power is adaptively distributed among the beams, i.e., if an FEADPAS replaces the FEADAS. This confirms the ability of the new faster adaptation algorithm to fully benefit from the transmitted power by optimally fitting the spots within the receiver's FOV and equally distributing the power

TABLE IV
SNR OF THE 15 GBIT/S RESTRICTED MULTIBEAM OW SYSTEMS

Configuration	SNR (dB)						
	Receiver locations along the *y*-axis, Y (m)						
	1	2	3	4	5	6	7
Restricted MBAPAS, (FOV = 4°)	-8.9	-7.9	-8.9	-7.9	-8.9	-7.9	-8.9
Restricted FEADPAS, (FOV = 4°)	17.2	18.3	17.2	18.3	17.2	18.3	17.2
Restricted FEADPAS, (FOV = 8°)	17.7	19.4	17.7	19.4	17.7	19.4	17.7

among the spots. In addition, a comparable SNR is observed in both MBAPAS and FEADPAS when the transmitted power is freely allocated to spots at key locations. However, the new system (FEADPAS) outperforms the previously proposed system (MBAPAS) if the total power is reduced below the current 1 W and a restriction is imposed on the algorithms to consider eye safety, so that no spot power exceeds 1 mW, which can help with eye safety at the near IR wavelengths [36]. Note that eye safety is not dictated in this case by the power per beam only, but also by the number of beams that can be seen simultaneously. Therefore further attention is needed to reduce the number of beams that can be seen simultaneously by considering the transmitter geometrical construction; however measures that can reduce the power per beam while maintaining the SNR are useful as proposed here. The SNR results of both systems (MBAPAS and FEADPAS in conjunction with a 4° diversity receiver), obtained through the use of an adaptation algorithm that restricts the power per beam to less than 1 mW, are given in Table IV. The SNR of FEADPAS with restricted per beam power (less than 1 mW per beam) with an 8° diversity receiver is also included. The results show that the per beam power can be maintained below 1 mW while achieving 10^{-9} BER at a bit rate of 15 Gbit/s where the new FEADPAS achieves an SNR of 17.4 dB, which is greater than the 15.6 dB needed. This SNR is obtained when using a 4° diversity receiver with 1 mm^2 detector area, and given the worst communication links studied where mobility, shadowing and signal blockage all exist.

IX. CONCLUSION

In this paper, we introduced a fast adaptation method to OW multibeam angle, power and delay adaptation systems and introduced a new spot diffusing geometry with beams clustered around the diversity receiver faces. The fast adaptation algorithm reduces the computations needed to reconfigure the transmitter in the case of transmitter and/or receiver mobility. The beam clustering approach provides the transmitter with the opportunity to allocate the power to spots within the receiver FOV and increases the number of such spots. Therefore if the power per spot is restricted to assist in meeting eye safety, then our new approach where more spots are visible within the receiver FOV leads to enhanced SNR. Note that if the power per beam is not restricted, then the new and previous systems we introduced have comparable performance as the total power can be allocated in the earlier system to the one (or few) spots within the receiver FOV.

The fast angle adaptation algorithm converges towards the optimum spot distribution that maximizes the receiver SNR through an efficient use of a divide and conquer algorithm. The results have also confirmed that while the original MBAAS benefits from power adaptation, power adaptation is not necessary when the new FEAAS is implemented. This is due to the ability of the new system to fully benefit from the transmitted power through optimizing the number and pattern (positions) of spots so as to maximize the receiver's SNR, regardless of the receiver's orientation and its FOV. The new system can also adapt to environmental changes, offering a link that is robust against shadowing and signal blockage through disregarding the obstructed spots and distributing the power equally among unobstructed spots. The new FEAAS offers an SNR improvement of 9 dB and reduces the computation cost by a factor of 20 compared to the original MBAAS.

Furthermore beam delay adaptation was introduced to FEAAS to mitigate the effect of multipath dispersion and ISI, and to improve system performance. The beam delay adaptation method can help the multibeam transmitter to adjust the switching times of the beams in a fashion that can allow the signals to reach the receiver at the same time. Significant improvements in the SNR with OW channel bandwidths of more than 15 GHz can be achieved, enabling the system to maintain higher data rates (15 Gbit/s and beyond). In addition, a restriction was imposed in the adaptation algorithm to limit the power per beam to less than 1 mW to assist with eye safety requirements. Note that eye safety is also a function of the number of beams that can be seen simultaneously by the eye. Future work will address the transmitter geometrical structure to examine these features.

ACKNOWLEDGMENT

The authors would like to acknowledge with thanks DSR technical and financial support.

REFERENCES

[1] F. R. Gfeller and U. H. Bapst, "Wireless in-house data communication via diffuse infrared radiation," *Proc. IEEE*, vol. 67, no. 11, pp. 1474–1486, Nov. 1979.
[2] J. M. Kahn and J. R. Barry, "Wireless infrared communications," *Proc. IEEE*, vol. 85, no. 2, pp. 265–298, Feb. 1997.
[3] S. Jivkova and M. Kavehard, "Multispot diffusing configuration for wireless infrared access," *IEEE Trans. Commun.*, vol. 48, no. 6, pp. 970–978, Jun. 2000.
[4] J. R. Barry, J. M. Krause, E. A. Lee, and D. G. Messerschmitt, "Simulation of multipath impulse response for indoor wireless optical channels," *IEEE J. Sel. Areas Commun.*, vol. 11, no. 3, pp. 367–379, Apr. 1993.
[5] K. Alkhavan, M. Kavehard, and S. Jivkova, "High-speed power-efficient indoor wireless infrared communication using code combining—Part I," *IEEE Trans. Commun.*, vol. 50, no. 7, pp. 1495–1502, Nov. 2002.
[6] A. G. Al-Ghamdi and J. M. H. Elmirghani, "Line strip spot-diffusing transmitter configuration for optical wireless systems influenced by background noise and multipath dispersion," *IEEE Trans. Commun.*, vol. 52, no. 1, pp. 37–45, Jan. 2004.
[7] A. G. Al-Ghamdi and J. M. H. Elmirghani, "Performance comparison of LSMS and conventional diffuse and hybrid wireless techniques in a real indoor environment," *IEE Proc. Optoelectron.*, vol. 152, no. 4, pp. 199–204, Aug. 2005.

[8] F. E. Alsaadi and J. M. H. Elmirghani, "High-speed spot diffusing mobile optical wireless system employing beam angle and power adaptation and imaging receivers," *J. Lightw. Technol.*, vol. 28, no. 16, pp. 2191–2206, Aug. 2010.
[9] M. A. Alhartomi, F. E. Alsaadi, and J. M. H. Elmirghani, "Mobile optical wireless system using fast beam angle, delay and power adaptation with angle diversity receivers," in *Proc. 14th Int. Conf. Transparent Opt. Netw.*, Jul. 2–5, 2012, pp. 1–5.
[10] M. T. Alresheedi and J. M. H. Elmirghani, "High-speed indoor optical wireless links employing fast angle and power adaptive computer-generated holograms with imaging receivers," *submitted to J. Lightw. Technol.*, to be published.
[11] M. T. Alresheedi and J. M. H. Elmirghani, "10 Gbit/s indoor optical wireless systems employing beam delay, power and angle adaptation methods with imaging detection," *J. Lightw. Technol.*, vol. 30, no. 12, pp. 1843–1856, Jun. 2012.
[12] D. O'Brien, R. Turnbull, H. L. Minh, G. Faulkner, O. Bouchet, P. Porcon, M. El Tabach, E. Gueutier, M. Wolf, L. Grobe, and J. Li, "High-speed optical wireless demonstrators conclusions and future directions," *J. Lightw. Technol.*, vol. 30, no. 13, pp. 2181–2187, Jul. 2012.
[13] G. Ntogari, T. Kamalakis, and T. Sphicopoulos, "Analysis of indoor multiple-input multiple-output coherent optical wireless systems," *J. Lightw. Technol.*, vol. 30, no. 3, pp. 317–324, Feb. 2012.
[14] T. Fath, C. Heller, and H. Haas, "Optical wireless transmitter employing discrete power level stepping," *J. Lightw. Technol.*, vol. 31, no. 11, pp. 1734–1743, Jun. 2013.
[15] K. Wang, A. Nirmalathas, C. Lim, and E. Skafidas, "4 × 12.5 Gb/s WDM optical wireless communication system for indoor applications," *J. Lightw. Technol.*, vol. 29, no. 13, pp. 1988–1996, Jul. 2011.
[16] H. Xu, B. Davey, D. Timothy, D. Wilkinson, and W. A. Crossland, "Optically enhancing the small electro-optical effect of a fast-switching liquid-crystal mixture," *Opt. Eng.*, vol. 39, no. 6, pp. 1568–1572, Jun. 2000.
[17] C. J. Henderson, D. G. Leyva, and T. D. Wilkinson, "Free space adaptive optical interconnect at 1.25 Gb/s, with beam steering using a ferroelectric liquid-crystal SLM," *J. Lightw. Technol.*, vol. 24, no. 5, pp. 1989–1997, May 2006.
[18] P. L. Eardley, D. R. Wisely, D. Wood, and P. McKee, "Holograms for optical wireless LANs," *IEE Proc. Optoelectron.*, vol. 143, no. 6, pp. 365–369, Dec. 1996.
[19] A. J. C. Moreira, R. T. Valadas, and A. M. De Oliveira Duarte, "Optical interference produced by artificial light," *Wireless Netw.*, vol. 3, no. 2, pp. 131–140, Dec. 1997.
[20] S. Zahedi, J. A. Salehi, and M. Nasiri-Kenari, "A photon counting approachto the performance aalysis of indoors wireless infrared CDMA networks," in *Proc. IEEE PIMRC'00*, London, U.K., 2000, vol. 2, pp. 928–932.
[21] A. C. Boucouvalas, "Indoor ambient light noise and its effect on wireless optical links," *IEE Proc. Optelectron.*, vol. 143, no. 6, pp. 334–38, Dec. 1996.
[22] P. Djahani and J. Kahn, "Analysis of infrared wireless links employing multibeam transmitter and imaging diversity receivers," *IEEE Trans. Commun.*, vol. 48, no. 12, pp. 2077–2088, Dec. 2000.
[23] W. T. Welford and R. Winston, *High Collection Nonimaging Optics*. San Diego, CA, USA: Academic, 1989.
[24] U. Weidmann, Transporttechnik der FussgNanger, Schriftenreihe des IVT, vol. 80, ETH, ZNurich, 1992.
[25] P. Viswanath, D. N. C. Tse, and R. Laroia, "Opportunistic beamforming using dumb antennas," *IEEE Trans. Inf. Theory*, vol. 48, no. 6, pp. 1277–1294, Jun. 2002.
[26] A. Legout, G. Urvoy Keller, and P. Michiardi, "Rarest first and choke algorithms are enough," in *Proc. 6th ACM SIGCOMM Conf. Internet Meas.*, New York, NY, USA, 2006, pp. 203–216.
[27] E. Desurvire, *Erbium-Doped Fiber Amplifiers: Principles and Applications*. New York, NY, USA: Wiley, 1994.
[28] J. M. H. Elmirghani, H. H. Chan, and R. A. Cryan, "Sensitivity evaluation of optical wireless PPM systems utilizing PIN-BJT receivers," *IEE Proc. Optoelectron.*, vol. 143, no. 6, pp. 355–359, Dec. 1996.
[29] J. Kleinberg and E. Tardos, *Algorithm Design*. Boston, MA, USA: Pearson Education, 2006.
[30] E. Kimber, B. Patel, and A. Hadjifotiou, "12 GHz PIN-HEMT optical receiver front end," *IEE Colloq. Opt. Detector Receivers*, pp. 701–710, Oct. 1993.
[31] S. D. Personick, "Receiver design for digital fiber optical communication system—Part I and II," *Bell Syst. Technol. J.*, vol. 52, no. 6, pp. 843–886, Jul./Aug. 1973.
[32] "10 Gb/s optical transponder" [Online]. (2011). Available: http://www.finisar.com/sites/default/files/pdf/12TRAAU4MALCB-10Gbs-Tunable-Long-Reach-Transponder-product-brief-RevF
[33] "MSA 10 Gb/s Transponder" (2005). [Online]. Available: http://www.fujitsu.com/downloads/OPTCMP/lineup/300msa/300msatdm-catalog
[34] G. W. Marsh and J. M. Kahn, "50-Mb/s diffuse infrared free-space link using on-off keying with decision-feedback equalization," *IEEE Photon. Technol. Lett.*, vol. 10, no. 6, pp. 1268–1270, Oct. 1994.
[35] G. W. Marsh and J. M. Kahn, "Performance evaluation of experimental 50-Mb/s diffuse infrared wireless link using on-off keying with decision-feedback equalization," *IEEE Trans. Commun.*, vol. 44, no. 11, pp. 1496–1504, Nov. 1996.
[36] A. C. Boucouvalas, "IEC 825–1 eye safety classification of some consumer electronic products," in *Proc. IEE Colloq. Opt. Free Space Commun. Links*, Feb. 19, 1996, pp. 13/1–13/6.

Fuad E. Alsaadi received the B.S. and M.Sc. degrees in electronic and communication from King AbdulAziz University, Jeddah, Saudi Arabia, in 1996 and 2002. He then received the Ph.D. degree in optical wireless communication systems from the University of Leeds, Leeds, U.K., in 2011. Between 1996 and 2005, he worked in Jeddah as a Communication Instructor in the College of Electronics and Communication. He was a Lecturer in the Faculty of Engineering, King AbdulAziz University in 2005. He is currently an Assistant Professor of the Departement of Electrical and Computer Engineering within the Faculty of Engineering, King Abdulaziz University. He published widely in the top IEEE communications conferences and journals and has received the Carter award, University of Leeds for the best Ph.D. His research interests include in optical systems and networks and signal processing.

Mohammed A. Alhartomi received the B.Sc. degree in electronic and communication engineering from King Abdul Aziz University, Jeddah, Saudi Arabia, in 2004 and the M.Sc. degree in communication systems from Swansea University, Swansea, U.K., in 2010. He is currently working toward the Ph.D. degree in electronic and electrical engineering.

Jaafar M. H. Elmirghani received the B.Sc. (First Class Hons.) in electrical engineering from the University of Khartoum, Sudan, in 1989 and the Ph.D. degree in 1994 from the University of Huddersfield, U.K., for work on optical receiver design and synchronization. He is a Fellow of the IET, Fellow of the Institute of Physics, and is the Director of the Institute of Integrated Information Systems and Professor of Communication Networks and Systems within the School of Electronic and Electrical Engineering, University of Leeds, U.K. He joined Leeds in 2007 and prior to that (2000–2007) as the Chair in optical communications at the University of Wales Swansea, he founded, developed, and directed the Institute of Advanced Telecommunications. He was the Chairman of the IEEE U.K. and RI Communications Chapter and was the Chairman of IEEE Comsoc Transmission Access and Optical Systems Committee andthe Chairman of IEEE Comsoc Signal Processing and Communication Electronics (SPCE) Committee. He was a member of IEEE ComSocTechnical Activities Council' (TAC), was an Editor of IEEE COMMUNICATIONS MAGAZINE and is and has been on the technical program committee of 29 IEEE ICC/GLOBECOM conferences between 1995 and 2012 including ten times as Symposium Chair. He was the founding Chair of the Advanced Signal Processing for Communication Symposium which started at IEEE GLOBECOM'99 and has continued since at every ICC and GLOBECOM. Dr. Elmirghani was also founding Chair of the first IEEE ICC/GLOBECOM optical symposium at GLOBECOM'00, the Future Photonic Network Technologies, Architectures, and Protocols Symposium. He chaired this Symposium, which continues to date. He received the IEEE Communications Society 2005 Hal Sobol award for exemplary service to meetings and conferences, the IEEE Communications Society 2005 Chapter Achievement award, the University of Wales Swansea inaugural 'Outstanding Research Achievement Award', 2006, the IEEE Communications Society Signal Processing and Communication Electronics outstanding service award, 2009, and all four prizes awarded by the University of Khartoum for academic distinction in the Department of Electrical Engineering. He is currently an Editor of *IET Optoelectronics*, Editor of *Journal of Optical Communications*, Cchair of the GreenTouch Core Switching and Routing Working Group, an adviser to the Commonwealth Scholarship Commission, member of the Royal Society International Joint Projects Panel and a member of the Engineering and Physical Sciences Research Council (EPSRC) College.